Title: Tracer studies to characterize the effects of roadside noise barriers on near-road pollutant dispersion under varying atmospheric stability conditions

Authors: Dennis Finn[1]*, Kirk L. Clawson[1], Roger G. Carter[1], Jason D. Rich[1], Richard M. Eckman[1], Steven G. Perry[2], Vlad Isakov[2], and David K. Heist[2]

Affiliations:
1 – Air Resources Laboratory, Field Research Division, National Oceanic and Atmospheric Administration, Idaho Falls, ID
2 – Atmospheric Modeling and Analysis Division, National Exposure Research Laboratory, U.S. Environmental Protection Agency, Research Triangle Park, NC

Sponsorship: This work was completed under Interagency Agreement DW-13-92274201-0 between the National Oceanic and Atmospheric Administration and the U.S. Environmental Protection Agency.

*Corresponding author
Dennis Finn
NOAA/ARLFRD
1750 Foote Drive
Idaho Falls, ID 83402
Ph: (208) 526-0566
Fax: (208) 526-2549
Email: dennis.finn@noaa.gov

Abstract

A roadway toxics dispersion study was conducted at the Idaho National Laboratory (INL) to document the effects on concentrations of roadway emissions behind a roadside sound barrier in various conditions of atmospheric stability. The homogeneous fetch of the INL, controlled emission source, lack of other manmade or natural flow obstructions, and absence of vehicle-generated turbulence reduced the ambiguities in interpretation of the data. Roadway emissions were simulated by the release of an atmospheric tracer (SF_6) from two 54 m long line sources, one for an experiment with a 90 m long noise barrier and one for a control experiment without a barrier. Simultaneous near-surface tracer concentration measurements were made with bag samplers on identical sampling grids downwind from the line sources. An array of six 3-d sonic anemometers was employed to measure the barrier-induced turbulence. Key findings of the study are: (1) the areal extent of higher concentrations and the absolute magnitudes of the concentrations both increased as atmospheric stability increased; (2) a concentration deficit developed in the wake zone of the barrier with respect to concentrations at the same relative locations on the control experiment at all atmospheric stabilities; (3) lateral dispersion was significantly greater on the barrier grid than the non-barrier grid; and (4) the barrier tended to trap high concentrations near the "roadway" (i.e. upwind of the barrier) in low wind speed conditions, especially in stable conditions.

Keywords:

wake zone, traffic emissions, pollutant dispersion near roadways, concentration deficits

1. Introduction

47 Vehicle-related toxic emissions from roadways include such pollutants as particulate
48 matter, carbon monoxide, heavy metals, and volatile organic compounds such as benzene.
49 Numerous studies have found that people living and working near roadways are exposed to
50 elevated levels of pollution and are at increased risk of respiratory problems (e.g., Nitta et al.,
51 1993; McConnell et al., 2006), birth and developmental defects (e.g., Wilhelm and Ritz, 2003),
52 premature mortality (e.g., Finkelstein et al., 2004; Jerrett et al., 2005), cardiovascular effects
53 (e.g., Peters et al., 2004; Riediker et al., 2004), and cancer (e.g., Harrison et al., 1999; Pearson et
54 al., 2000). Given that noise barriers and vegetation are now common roadside features it is
55 pertinent to ask what effect they might have on pollution levels adjacent to roadways.
56 Many studies have looked at the effects of roadside noise barriers on pollution levels in
57 adjacent areas. Some of these studies suggest that, for gaseous pollutants, a barrier results in a
58 well-mixed zone with lower concentration extending downwind behind the barrier (Baldauf et
59 al., 2008; Nokes and Benson, 1984; Paul-Carpenter and Barboza, 1988; Hõlscher et al., 1993;
60 Bowker et al., 2007). Depending upon roadway plus barrier configuration, concentration deficits
61 of 50% or more have been observed relative to a reference roadway configuration without a
62 barrier. These concentration deficit regions can extend in excess of 20 wall heights downwind
63 (Heist et al., 2009). The low concentration region has been attributed to upward deflection of the
64 airflow and increased vertical mixing due to the barrier as well as enhanced initial mixing due to
65 turbulence on the roadway generated by traffic. For heavy metals such as lead, a barrier will
66 inhibit downwind transport and result in increased deposition in the roadway area (Swamy and
67 Lokesh, 1993).
68 Several studies have also examined the role of roadside vegetation (Bowker et al., 2007;
69 Beckett et al., 2000; Bussotti et al., 1995; Heath et al., 1999; Heichel and Hankin, 1976; Munch,

70 1993; Tan and Lepp, 1977: Swamy and Lokesh, 1993; Madders and Lawrence, 1985). These
71 studies suggest that vegetation also reduced downwind pollutant concentrations by enhancing
72 mixing and dispersion as well as increased the deposition of some species (e.g. heavy metals) in
73 the immediate roadway area.

74 Despite the accumulating evidence, uncertainties regarding the effects of roadside noise
75 barriers on pollutant concentrations in surrounding areas remain. Specifically, the role of
76 atmospheric stability has not been investigated in any systematic manner. Most wind tunnel
77 studies are done in neutral stability conditions and most of the field experimental work has been
78 done during the daytime. Furthermore, much of the field work has been done in "natural"
79 settings featuring moving traffic and the associated turbulence, variations in source strength, and
80 irregular distributions of flow obstructions. All of these can considerably complicate the
81 interpretation of results.

82 The Field Research Division (FRD) of the Air Resources Laboratory (ARL) of the
83 National Oceanic Atmospheric Administration (NOAA) conducted the Near Roadway Tracer
84 Study (NRTS08) during October 2008. The work was sponsored by the Atmospheric Modeling
85 and Analysis Division of the U.S. Environmental Protection Agency (EPA). NRTS08 was
86 designed to quantify the effects of roadside barriers on the downwind dispersion of atmospheric
87 pollutants emitted by roadway sources (e.g. vehicular transport). Pollutant transport and
88 dispersion were measured during the field tests using sulfur hexafluoride (SF_6) tracer gas as a
89 pollutant surrogate. The turbulence field driving the dispersion was also measured. The goal of
90 the study was to produce a roadway barrier dataset that (1) covered a range of atmospheric
91 stabilities, (2) minimized factors that could complicate data interpretation, and (3) could be used

92 to guide further development of models such as AERMOD (Cimorelli et al., 2005) to simulate
93 the effects of roadway emissions.

94 2. Methods

95 The field study was done near NOAA's Grid 3 diffusion grid at the Department of
96 Energy's Idaho National Laboratory (INL). The Grid 3 area on the INL was selected for
97 NRTS08 for a number of reasons. The INL is located across a broad, relatively flat plain on the
98 western edge of the Snake River Plain in southeast Idaho. The Grid 3 area was originally
99 designed to conduct transport and dispersion tracer studies in the 1950s. It is part of the INL
100 mesonet (Clawson et al., 2007). Numerous tracer and other atmospheric studies have been
101 conducted at Grid 3 since that time (Start et al. 1984; Sagendorf and Dickson, 1974; Garodz and
102 Clawson, 1991, 1993). Conducting NRTS08 at Grid 3 allowed for optimal control of the
103 experimental configuration, in particular, the need for having the roadway and barrier oriented
104 perpendicular to the wind direction. This control increased the chances of obtaining high quality
105 measurements that would be of the greatest benefit toward the goal of improving model
106 reliability. The general selection of the site and timing for the experiments were also guided by
107 historical wind rose data generated by the NOAA-INL mesonet to afford the maximum
108 opportunity for the realization of ideal wind direction conditions. The open, level terrain without
109 other manmade or natural obstructions or complexities also made the data easier to interpret.

110 Five tests were conducted during NRTS08, each spanning a 3-h period broken into 15-
111 min tracer sampling intervals. One test was conducted in unstable conditions, one in neutral
112 conditions, and three in stable conditions. All lengths and distances in the study were referenced
113 to multiples of the barrier height H. A 90 m long (15H) by 6 m high (1H = 6 m) straw bale stack
114 represented a roadway barrier for the primary experiment (Fig. 1). The "roadway" itself was

115 nothing more than an access track through the sagebrush adjacent to the barrier. The primary
116 and reference control experiments both had a 54 m long (9H) SF_6 tracer line source release
117 positioned 1 m above ground level (AGL) representing pollution sources from a roadway on the
118 upwind side of the barrier and a gridded array of bag samplers downwind of the line source and
119 barrier for measuring mean 15-min concentrations (Fig. 2). An array of six 3-d sonic
120 anemometers was deployed for making wind and turbulence measurements, 5 on the primary
121 experiment and 1 on the control experiment (Fig. 3). The barrier was oriented at 303 degrees
122 azimuth in order to be approximately perpendicular to the prevailing SSW winds during the day
123 and NE drainage flows at night. It was located 1H downwind of the line source so that the
124 source represented the median for a virtual 2-lane roadway 2H in width, including shoulders.
125 The barrier was 36 m longer than the line source in an attempt to minimize barrier edge effects,
126 i.e., tracer leaking around the barrier.
127 Approx. location Figs. 1-3
128 The primary and control experimental sampling grids had a large crosswind separation of
129 about 700 m at the point of closest proximity between the edges of the two grids to eliminate
130 possible interferences. Each sampling grid was composed of two sub-grids, one NE of the
131 release line and one SW of the release line. The NE sub-grid was used for SW winds and the
132 SW sub-grid was used for NE winds. The origin for the grid coordinate system was the midpoint
133 of the line source release with x positive in the streamwise direction, perpendicular to the barrier,
134 the y-axis was along the line source, and the positive z-direction was vertically upwards.
135 The location of the sonic anemometers was governed by: (1) the need to measure the
136 upwind approach flow, (2) the need to measure the turbulence field as close as practical to the
137 line source, and (3) the importance of measuring the turbulence field in the wake region of the

138 barrier where the greatest changes in the concentration and turbulence fields were expected to
139 occur. One anemometer was located -1.6H upwind of the line source on the control experiment
140 at a height of 3 m (0.5H) and served as a reference for the approach flow. Another anemometer
141 was located -1.6H upwind of the line source on the primary experiment at a height of 0.5H for
142 measuring turbulence in the tracer release area and the effects of the barrier on the approach
143 flow. Three anemometers were located on a tower 4H downwind of the release at heights of 3,
144 6, and 9 m (0.5, 1, 1.5H, respectively) to provide a vertical profile of the flow and turbulence
145 through and above the barrier wake region. A fourth was located farther downwind at 11H near
146 the estimated flow reattachment zone. Five of the sonics were R. M. Young Model 81000
147 Ultrasonic Anemometers and one was a Gill Windmaster Pro Anemometer. An additional suite
148 of supplemental meteorological measurements were made on the INL mesonet and at a 30 m
149 tower located between the two grids (Clawson et al., 2009).

150 Each of the two sampling grids had 58 sampler locations marked by metal fence posts.
151 The design of the grids was patterned after the work of Heist et al. (2009), to provide a basis for
152 intercomparison of near-neutral data, and guided by considerations of where the greatest changes
153 in the concentration field were expected. Heist et al. (2009) indicated that the largest alongwind
154 concentration gradients and greatest differences between the barrier and flat terrain cases in wind
155 tunnel studies occurred within the first 10-15H. For this reason, sampler density was greatest
156 near the barrier and decreased in the downwind direction (Fig. 2). Two of the samplers were
157 deployed upwind of the release line at x = -1H and x= -2H to check for possible upwind tracer
158 dispersion. All bag samplers were attached to the metal fence posts at approximately 1.5 m AGL.
159 In addition to the 58 regular samplers on each grid, an additional 9 samplers were deployed for
160 quality control purposes. These included field duplicates, field controls, and field blanks.

161 The SF_6 bag samplers housed a microprocessor and 12 microprocessor-controlled air
162 pumps designed to sequentially fill sample bags for a specified time and duration. Sampler
163 cartridges loaded with 12 Tedlar® bags were installed in the samplers and each bag was filled
164 for 15 min. Bag samples were analyzed using gas chromatography at the FRD Tracer Analysis
165 Facility in Idaho Falls, Idaho. A complete description of the analytical procedures and rigorous
166 quality control procedures used are described in Clawson et al. (2005, 2009). The data reported
167 are accurate to within +/-20% of NIST-certified standards and, with very few exceptions, are
168 accurate within +/-10%.
169 A single tracer line source was used to simulate roadway emissions for the primary and
170 control experimental grids. The tracer release system was engineered to simultaneously release
171 SF_6 from two independently controlled release systems and dissemination lines, one for each grid
172 (Fig. 4). This permitted measurement of barrier and non-barrier dispersion effects under
173 identical meteorological conditions. During tracer releases, gaseous SF_6 tracer flowed from
174 small (about 8 kg) aluminum cylinders containing liquid SF_6, through calibrated mass flow
175 controllers, and into flexible 0.125 inch (3.175 mm) inside diameter polyurethane tubes
176 connected to the two 54 m long release lines. The flow controllers provided temporal flow
177 consistency of better than 1% over the duration of each release period. The absolute accuracy of
178 the mass flow controllers was ±2% of full scale. Uniform flow across the line was assured by
179 maintaining equal pressure drop at each of 64 equally spaced release points on each line. The
180 release points were 31-gage hypodermic needles. Equal pressure drop was maintained by
181 supplying tracer gas using a 6-level binary network and equal lengths of tubing to divide the flow
182 to each of the needles. Rotameter flow measurements at each needle confirmed uniform flow
183 across each line within ±10% prior to each test.

184 Approx. location Fig. 4

185 The mass flow controller measurements of SF_6 were checked against the total mass
186 released. The total mass of SF_6 released for each test on the two release lines was determined
187 using the beginning and ending weight of the SF_6 cylinders as measured by a precision Ohaus
188 AV8101 electronic scale for each of the two bottles. These scales were capable of weighing up
189 to 8100 g with a resolution of 0.1 g and a full range accuracy of 0.4 g. The scale calibration was
190 checked prior to each release. Known weights were placed on the scale along with the SF_6
191 cylinder still attached. It was found that the scale was within the 0.4 g manufacturer
192 specification on all tests. With the overall accuracy of the scale being 0.4 g and the smallest total
193 release during a test being 269 g of SF_6, the maximum uncertainty of SF_6 released during a test
194 was less than 0.15 percent. Additional details on the line source are provided in Clawson et al.
195 (2009).

196 The SF_6 tracer was simultaneously released from the line source for each grid beginning
197 15 min before the sampler measurements started to establish a quasi-steady state concentration
198 field and continued until the end of each test. Tracer release rates ranged from 0.02 to 0.05 g s^{-1}.

199 3. Results

200 A brief summary of meteorological conditions during the individual tests follows. The
201 assignment of atmospheric stability for the cases used in the analysis (Table 1) was based upon
202 the z/L value calculated from the turbulence measurements at the 3-d sonic located -1.6H upwind
203 of the non-barrier release line.

204 Approx. location Table 1

205 Test 1 was conducted on October 9, 2008 from 1230-1530 hours Mountain Standard
206 Time (MST) in neutral stability conditions. Meteorological conditions were nearly ideal for this

stability condition. Winds were generally well in excess of 5 m s^{-1} and skies were heavily overcast. In fact, a light snow was falling during the experimental setup and continued for about a half hour after the start of the experiment. The overcast gradually dissipated during the last hour and a half of the experiment but conditions were very close to neutral throughout.

Test 2 was conducted on October 17, 2008 from 1300-1600 hours MST in unstable conditions. Winds were very light and variable prior to the start of the test but a forecast for light SW winds developing at the experimental site informed the decision to proceed with the test. In fact, the wind field did eventually become organized and consistent light SW winds set up shortly after the test started. The mean wind direction was mostly favorable although there was considerable variability in wind direction, as would be expected in light wind conditions. Skies were clear and sunny throughout the test period. In combination with the light winds, the situation provided a very favorable representation of unstable conditions.

Test 3 was conducted on October 18, 2008 from 1600-1900 hours MST in weakly stable conditions. The wind direction was very close to ideal until the last hour of the experiment when a transition in the wind field occurred. Skies were clear throughout the experiment.

Test 4 was conducted in moderately to strongly stable conditions but was not used because the wind direction was unfavorable with respect to the barrier orientation.

Test 5 was conducted on October 24, 2008 from 1800-2100 hours MST in moderate to strongly stable conditions. At the start of sampling the skies over the experimental site were approximately 70% covered by high cirrus. These thinned throughout the test period and the skies were mostly clear by the end. Winds were generally favorable until the last hour of the experiment.

229 The key results from NRTS08 can be seen in Figs. 5-9. Figures 5-7 show results for
230 selected representative 15-min periods for unstable to stable conditions. Figures 8 and 9 show
231 mean results for all 15-min periods satisfying certain wind direction constraints for each stability
232 condition.

233 Approx. location Figs. 5, 6, 7

234 The maps in Fig. 5 are arrayed in a 4 by 2 matrix. From top to bottom, the rows are
235 representative selections for unstable, neutral, weakly stable, and strongly stable 15-min periods
236 (Tests 2, 1, 3, and 5, respectively). The left column shows results for the control non-barrier grid
237 and the right column shows results for the matching primary grid with barrier. The
238 concentrations c have been normalized by the tracer release rate Q, wind speed u, line source
239 length L_y, virtual roadway width L_x, and the density ρ of SF_6 corrected for local pressure and
240 temperature to better facilitate comparison between all of the tests ($\chi = cL_xL_y\, u\rho/Q$). Wind
241 vector coordinates have all been transformed such that wind directions are plotted with reference
242 to the grid centerline, not standard meteorological convention. Wind vectors are coded by height
243 z: black = 3 m; light blue = 6 m; and red = 9 m. The wind scale vector below the normalized
244 concentration legend provides a wind speed reference of 2 m s^{-1} and indicates true north with
245 respect to the sample grids. Wind speeds less than 0.4 m s^{-1} are indicated by a '+'. The tracer
246 release line is indicated by a red line at x = 0 and the barrier is indicated by a bold black line at x
247 = 1H. Table 1 is a corresponding summary of the meteorology for each of the selections shown.

248 The first obvious feature of Fig. 5 is that the areal extent of higher concentrations and the
249 absolute magnitudes of the concentrations both increased as atmospheric stability increased.
250 This was true for both the primary and control experimental grids. Second, lateral dispersion and
251 horizontal plume spread were significantly greater on the barrier grid than the non-barrier control

252 grid. Plumes on the non-barrier grid tended to be narrower with sharper, better defined
253 boundaries as opposed to the more diffuse and lower concentration gradient patterns observed on
254 the barrier grid.

255 Third, the barrier tended to trap high concentrations in the "roadway" (i.e. upwind of the
256 barrier) in low wind speed conditions. In particular, very high concentrations were trapped in the
257 "roadway" in stable, low wind speed conditions (Fig. 5h). In fact, the highest concentrations
258 measured during NRTS08 were at the samplers upwind of the line source on the barrier grid in
259 stable conditions. This situation might constitute a health concern for people on the roadway.

260 Fourth, the barrier decelerated and deflected the approach flow. This can be seen by
261 comparing the approach flow wind vector for the control experiment with its counterpart upwind
262 of the barrier (Figs. 5 and 6).

263 Finally, there was a concentration deficit in the wake zone of the barrier with respect to
264 concentrations at the same grid locations on the non-barrier side for all atmospheric stabilities.
265 Figure 7 emphasizes this point by showing the results of dividing the barrier concentration by the
266 non-barrier concentration at each corresponding grid location, i.e. the ratio between the barrier
267 and non-barrier concentrations, for each of the selected representative cases. A large
268 concentration deficit region is apparent in each case. The deficit region usually extended beyond
269 the end of the grid at $x = 30H$ although it gradually diminished. Concentrations in the wake zone
270 of the barrier were typically less than 50% of their non-barrier equivalent and often less than
271 20%. The magnitude and areal extent of the concentration deficit was larger than that found in
272 some earlier studies for winds perpendicular to the roadway (e.g., Baldauf et al., 2008;
273 McNabola et al., 2009) but similar to other studies (Heist et al., 2009, cases A versus H).

274 The representative cases shown are a qualitative overview of the effects of barriers in
275 varying atmospheric stabilities for which the approach flow was approximately perpendicular to
276 the barrier. A more quantitative look at the data is shown in Fig. 8. It compares the normalized
277 concentration means and standard deviations for all 15-min periods where the mean reference
278 (control) wind direction was within 20 degrees of the centerline azimuth and the σ_θ values were
279 less than 35 degrees for the unstable, neutral, weakly stable, and strongly stable tests. These
280 constraints were set to minimize the influence of edge effects on centerline samplers downwind
281 due to finite line source length. Results are shown for both centerline and maximum crosswind
282 values for each downwind distance, the latter to better account for possible finite line source
283 edge effects.

284 The neutral and weakly stable tests show a sharp distinction between the primary and
285 control experiments with very small standard deviations (Figs. 8c-f). The distinction is less clear
286 for the unstable and stable tests although the means are distinctly different and there is very little
287 overlap of the one standard deviation error bars for the barrier and non-barrier curves (Figs. 8a,
288 b, g, h). The large discrepancy between the maximum and centerline values for the stable
289 condition barrier curves (compare Figs. 8 g, h) reflects barrier edge effects like those seen in Fig.
290 5h. Figure 9 plots the average barrier/non-barrier ratios along the centerline for the same periods
291 and makes obvious that the wake zone concentration deficit region is common to all stabilities.

292 Approx. location Figs. 8, 9

293 There is good agreement between tightly controlled wind tunnel experimental data (Heist
294 et al., 2009) and NRTS08 results for a similar configuration in neutral stability conditions (Fig.
295 10). The data shown were adjusted to represent an infinite line source using the technique
296 described in Heist et al. (2009). The comparison is affected by (1) there was one line source for

297 the NRTS08 field data and a 6 line source configuration for the wind tunnel experiments; (2) the
298 wind tunnel line sources were set into the plane of the surface while the line source in the field
299 was at 1 m AGL; and (3) the wind tunnel tracer measurements were made at the surface while
300 the field measurements were made at 1.5 m AGL. By fitting a curve to the field results for a
301 single line source and virtually shifting the position of the single line source to match the 6 line
302 source positions, it was found that the calculated differences between the sum of the 6 sources
303 versus a single source for χ were less than 5% for all $x < 30H$. The discrepancies in χ at smaller
304 values of x are probably attributable to the differences in release and sampling heights. The
305 elevated field release, in particular, would promote quicker mixing and dilution relative to a
306 surface source.

307 The large barrier/non-barrier concentration ratios in Fig. 7 along the flanks of the grid
308 probably represent some combination of barrier-enhanced plume spread and edge effects. The
309 magnitude of the discrepancy in the flanking zones was sometimes deceptive, however. In many
310 cases it involves a comparison between concentrations of as little as a few tens pptv on the
311 barrier grid to background concentrations of only 6-8 pptv on the non-barrier grid while the
312 concentrations toward the centerline of the grids were several thousands and even tens of
313 thousands pptv. The narrower non-barrier plumes certainly contributed to the high flanking
314 ratios.

315 For the representative 15-min test periods shown in Fig. 5, barrier edge effects were
316 negligible in Tests 1 and 3, are apparent in Test 2, and significant in Test 5. This pattern was
317 common for the other 15-min periods of Tests 1, 2, 3, and 5. The development of these edge
318 effects was related to mean wind direction, the extent of wind meander, wind speed, and
319 atmospheric stability. Lower wind speeds and/or the damped vertical motions and turbulence

320 associated with increased atmospheric stability contributed significantly to the development of
321 barrier edge effects. In the case of Test 5, the obvious effects of stability made it likely that
322 some tracer leakage would occur in the absence of a very long barrier.
323 Approx. location Fig. 10
324 Some key wind field and turbulence measurements provided by the 6 sonic anemometers
325 for each of the selected representative periods are summarized in Table 2 and Fig. 6. One
326 important observation is the clear evidence for a recirculation eddy in the wake zone. The wind
327 directions at x = 4H, z = 3 m were approximately 180 degrees of the approach flow in Tests 1, 3,
328 and 5. The wind directions at x = 4H, z = 6 m are also nearly opposite those of the approach
329 flow in Tests 1 and 3. Tests 1, 3, and 5 also show clear evidence of a zone of much higher
330 turbulence above the height of the barrier in the wake zone (x = 4H, z = 9 m) overlying a zone of
331 much lower turbulence at z = 3 m, and sometimes z = 6 m. This can be attributed to shear-
332 generated turbulence across the top of the barrier. Finally, the evidence is somewhat mixed on
333 whether x = 11H was far enough downwind to be beyond the reattachment point of the flow. It
334 appears as if the flow had not fully re-equilibrated with the approach flow in most respects at this
335 distance downwind. This was expressed by the lower wind speeds and/or turning of the wind
336 vector often observed there relative to the reference anemometer. Again, while there is
337 considerable variability between 15-min periods within a test, the observations represented by
338 the selected cases are common in the data set as a whole.
339 Approx. location Table 2
340 Test 2, the unstable case, had the least well-defined, shear-generated, high turbulence
341 zone although it had the highest normalized TKE (Fig. 6). The wind and turbulence fields
342 appeared to be more homogeneous than in the other tests. The recirculation eddy was also less

well-defined with the wind direction often more turned at a sharp angle rather than being completely 180 degrees reversed.

The simplest explanations for the observed concentration patterns are that (1) the tracer plume was forced to move up and over the barrier, enhancing plume dispersion in the vertical and lowering concentrations behind the barrier; and (2) the plume was forced to spread horizontally when the approach flow was decelerated and deflected by the barrier. The former would have had the additional effect of creating an elevated source. Once the tracer plume was lifted to the top of the barrier, its dispersion would be further enhanced in a highly turbulent shear zone, further decreasing downwind concentrations.

In low wind speed conditions, it was common for the tracer to be at least partly impounded and trapped in a low wind speed region in front of the barrier. Once trapped, turbulent diffusion often transported some of the tracer back to the samplers upwind of the line source. This effect was exaggerated during more strongly stable conditions (Test 5). With upward motion suppressed by very low turbulence levels, the tracer was not readily able to make it over the barrier. Much of the tracer then migrated to the edges of the barrier before being transported downwind. It is possible that turbulence generated by vehicular traffic in a real world setting would somewhat mitigate this trapping effect although high roadway mixing zone concentrations have been observed in such settings (Nokes and Benson, 1984).

4. Conclusions

The areal extent of higher concentrations and the absolute magnitudes of the concentrations both increased as atmospheric stability increased on both the primary and control experimental grids. Lateral dispersion and horizontal plume spread were significantly greater on

366 the barrier grid than the non-barrier grid. Plumes on the non-barrier control grid tended to be
367 narrower and have sharper and better defined boundaries as opposed to the more diffuse and
368 lower concentration gradient patterns observed on the barrier grid. There was a concentration
369 deficit in the wake zone of the barrier with respect to concentrations at the same grid locations on
370 the non-barrier side at all atmospheric stabilities. The areal extent of the deficit region varied
371 most in unstable or stable conditions featuring low wind speeds. The reduction in concentration
372 was typically in excess of 50% and often much greater. The barrier tended to trap high very
373 concentrations in the "roadway" (i.e. upwind of the barrier) in stable, low wind speed conditions.
374 This might be cause for potential human health concerns in some circumstances.

375 The barrier decelerated and deflected the approach flow. A well-defined recirculation
376 zone with low turbulence was usually present in the wake of the barrier. It tended to be more
377 poorly defined in unstable conditions. The recirculation zone was capped by a highly turbulent
378 region generated by shear across the top of the barrier. In most cases, the flow downwind of the
379 barrier at $x = 11H$, $z = 3$ m was not fully re-equilibrated with the approach flow.

380
381 Acknowledgments
382
383 We wish to thank Tom Pierce, Alan Vette, S.T. Rao, and David Mobley from the EPA
384 and Randy Johnson, Shane Beard, Tom Strong, Brad Reese, and Neil Hukari from FRD for the
385 contributions they made to NRTS08.
386
387 Disclaimer
388
389 The United States Environmental Protection Agency through its Office of Research and
390 Development funded and managed the research described here under Interagency Agreement
391 DW-13-92274201-0 with the National Oceanic and Atmospheric Administration. It has been
392 subjected to EPA and NOAA review and approved for publication although it does not
393 necessarily reflect their policies or views.

395 References
396
397 Baldauf, R.W., Thoma, E., Khlystov, A., Isakov, V., Bowker, G., Long, T., Snow, R., 2008.
398 Impacts of noise barriers on near-road air quality. Atmospheric Environment 42, 7502-
399 7507.
400
401 Beckett, J.P., Freer-Smith, P.H., Taylor, G., 2000. Effective tree species for local air quality
402 management. Arboricultural Journal 26 (1), 12-19.
403
404 Bowker, G.E., Baldauf, R., Isakov, V., Khlystov, A., Petersen, A., 2007. The effects of roadside
405 structures on the transport and dispersion of ultrafine particles from highways.
406 Atmospheric Environment 41, 8128-8139.
407
408 Busotti, F., Grossomi, P., Ferretti, M., Cenni, E., 1995. Preliminary studies on the ability of
409 plant barriers to capture lead and cadmium of vehicular origin. Aerobiologia 11 (1), 11-
410 18.
411
412 Cimorelli, A., Perry, S., Venkatram, A., Weil, J., Paine, R., Wilson, R., Lee, R., Peters, W.,
413 Brode, R., 2005. AERMOD: A dispersion model for industrial source applications. Part I:
414 General model formulation and boundary layer characterization. Journal of Applied
415 Meteorology 44, 682-693.
416
417 Clawson, K. L., Carter, R.G., Lacroix, D.J., Biltoft, C.A., Hukari, N.F., Johnson, R.C., Rich,
418 J.D., Beard, S.A., Strong, T., 2005. Joint Urban 2003 (JU03) SF_6 Atmospheric Tracer
419 Field Tests, NOAA Technical Memorandum OAR ARL-254, Air Resources Laboratory,
420 Idaho Falls, ID.
421
422 Clawson, K.L., Eckman, R.M., Hukari, N.F., Rich, J.D., Ricks, N.R., 2007. Climatography of
423 the Idaho National Laboratory 3rd Edition. NOAA Technical Memorandum OAR ARL-
424 259, Air Resources Laboratory, Idaho Falls, ID.

425 Clawson, K.L., Eckman, R.M., Johnson, R.C., Carter, R.G., Finn, D., Rich, J.D., Hukari, N.F.,
426 Strong, T., Beard, S.A., Reese, B.R., 2009. Near Roadway Tracer Study (2008). NOAA
427 Technical Memorandum OAR ARL-260, Air Resources Laboratory, Idaho Falls, Idaho.

428 EPA, 2000. Meteorological Monitoring Guidance for Regulatory Modeling Applications. EPA-
429 454/R-99-005, 171 pp.
430
431 Finkelstein, M.M., Jerrett, M., Sears, M.R., 2004. Traffic related air pollution and mortality rate
432 advancement periods. American Journal of Epidemiology 160(2), 173-177.
433
434 Garodz, L. J., Clawson, K.L., 1991. Vortex Characteristics of C5A/B, C141B, and C130E
435 aircraft applicable to ATC terminal flight operations, tower fly-by data.
436 NOAA/ERL/ARLFRD, Idaho Falls, Idaho, 250 pp.
437

438 Garodz, L. J., Clawson, K.L., 1993. Volume 1, Vortex Wake Characteristics of B757-200 and
439 B767-200 Aircraft Using the Tower Fly-By Technique. Volume 2, Appendices.
440 NOAA/ERL/ARLFRD, Idaho Falls, ID. 160 & 570 pp.
441
442 Harrison, R.M., Leung, P.L., Somerville, L., 1999. Analysis of incidence of childhood cancer in
443 the West Midlands of the United Kingdom in relation to the proximity of main roads and
444 petrol stations. Journal of Occupational and Environmental Medicine 56, 774-780.
445
446 Heath, B.A., Maughan, J.A., Morrison, A.A., Eastwood, I.W., Drew, I.B., Lofkin, M., 1999. The
447 influence of wooded shelterbelts on the deposition of copper, lead, and zinc at Shakerley
448 Mere, Cheshire, England. Science of the Total Environment 235, 415-417.
449
450 Heichel, G.H., Hankin, L., 1976. Roadside coniferous windbreaks as sinks for vehicular lead
451 emissions. Journal of the Air Pollution Control Association 26 (8), 767-770.
452
453 Heist, D. K., Perry, S.G., Brixey, L.A., 2009. A wind tunnel study of the effect of roadway
454 configurations on the dispersion of traffic-related pollution. Atmospheric Environment
455 43, 5101-5111.
456
457 Hõlscher, N., Hoffer, R., Niemann, H.-J., Brilon, W., Romberg, E., 1993. Wind tunnel
458 experiments on micro-scale dispersion of exhausts from motorways. Science of the Total
459 Environment 134, 71-79.
460
461 Jerrett, M., Burnett, R., Pope, C.A., 3rd, Krewski, D., Newbold, K.B., Thurston, G., Shi, Y.,
462 Finkelstein, N., Calle, E.E., Thun, M.J., 2005. Spatial analysis of air pollution and
463 mortality in Los Angeles. Epidemiology 16, 727-736.
464
465 Madders, M., Lawrence, M., 1985. The contribution made by vegetation buffer zones to
466 improved air quality in urban areas. In: Hall, D.O., Myers, N., Margaris, N.S. (Eds.),
467 Economics of Ecosystems Management, Dr. W. Junk Publishers, Dordrecht, Netherlands
468 ISBN 90-6193-505-9.
469
470 McConnell, R., Berhane, K., Yao, L., Jerrett, M., Lurmann, F., Gilliland, F., Kuenzli, N.,
471 Gauderman, J., Avol, E., Thomas, D., Peters, J., 2006. Traffic, susceptibility, and
472 childhood asthma. Environmental Health Perspectives 114, 766-772.
473
474 McNabola, A., Broderick, B.M., Gill, L.W., 2009. A numerical investigation of the impact of
475 low boundary walls on pedestrian exposure to air pollutants in urban street canyons.
476 Science of the Total Environment 407, 760-769.
477
478 Munch, D., 1993. Concentration profiles of arsenic, cadmium, chromium, copper, lead, mercury,
479 nickel, zinc, vanadium, and PAH in forest soil beside an urban road. Science of the Total
480 Environment 138, 7-55.
481
482 Nitta, H., Sato, T., Nakai, S., Maeda, K., Aoki, S. and Ono, M., 1993. Respiratory health

associated with exposure to automobile exhaust I. Results of cross-sectional studies in 1979, 1982, and 1983. Archives of Environmental Health 48, 53-58.

Nokes, W.A., Benson, P.E., 1984. Carbon monoxide concentrations adjacent to sound barriers. Office of Transportation Laboratory, California Department of Transportation, Report FHWA/CA/TL-84/04.

Paul-Carpenter, S., Barboza, M.J., 1988. Effects of highway noise barriers on carbon monoxide levels. In: 81st Annual meeting of the Air Pollution Control Association (APCA), Dallas, TX, June, 1988.

Pearson, R.L., Wachtel, H., Ebi, L., 2000. Distance-weighted traffic density in proximity to a home is a risk factor for leukemia and other childhood cancers. Journal of the Air and Waste Management Association 50, 175-180.

Peters, A., von Klot, S., Heier, M., Trentinaglia, I., Hormann, A., Wichmann, E., Lowel, H., 2004. Exposure to traffic and the onset of myocardial infarction. New England Journal of Medicine 351, 1721-1730.

Riediker, M., Cascio, W.F., Griggs, T.R., Herbst, M.C., Bromber, P.A., Neas, L., Williams, R., Devlin, R.B., 2004. Particulate matter exposure in cars is associated with cardiovascular effects in healthy, young men. American Journal of Respiratory and Critical Care Medicine 169, 934-940.

Sagendorf, J. F., Dickson, C.R., 1974. Diffusion under low windspeed, inversion conditions. NOAA Technical Memo ERL ARL-52, Air Resources Laboratory, Idaho Falls, ID.

Start, G.E., Sagendorf, J.F., Ackermann, G.R., Cate, J.H., Hukari, N.F., Disckson, C.R., 1984. Idaho Field Experiment 1981, Volume II: Measurement data, NUREG/CR-3488, Vol. 2, Air Resources Laboratory, Idaho Falls, ID.

Swamy, K.T.V., Lokesh, K.S., 1993. Lead dispersion studies along highways. Indian Journal of Environmental Health 35 (33), 205-209.

Tan, K.T., Lepp, N.W., 1977. Roadside vegetation: an efficient barrier to the lateral spread of atmospheric lead? Arboricultural Journal 3 (2), 79-85.

Wilhelm, M., Ritz, B., 2003. Residential proximity to traffic and adverse birth outcomes in Los Angeles County, California, 1994-1996. Environmental Health Perspectives 111, 207-216.

Figure 1

526

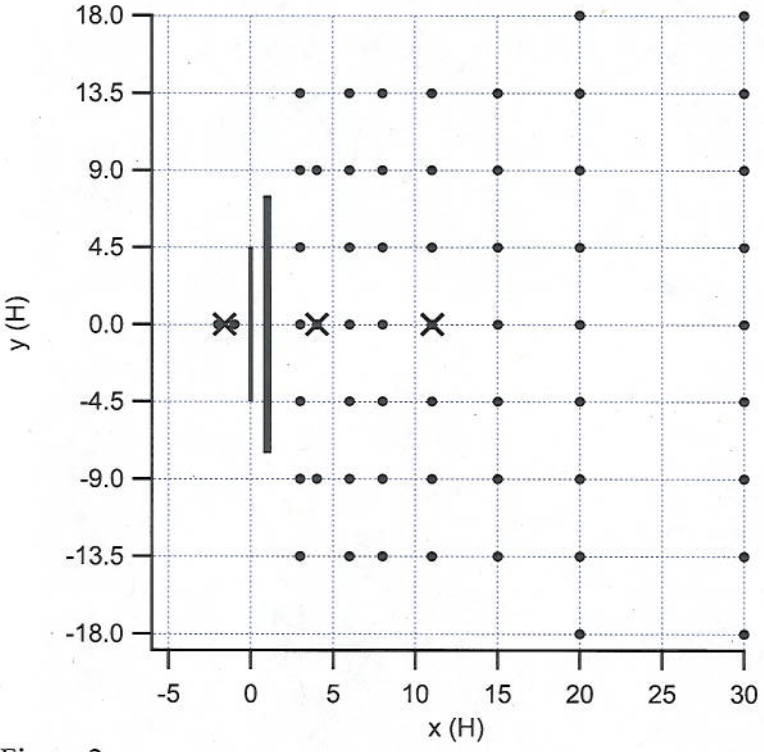

527

528 Figure 2

Figure 3

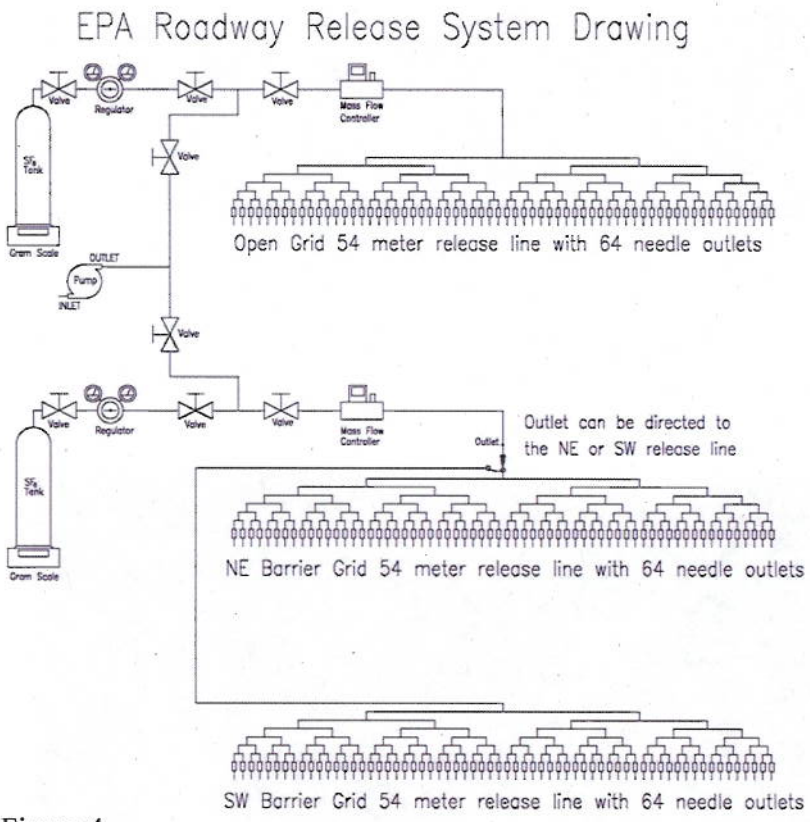

531
532 Figure 4

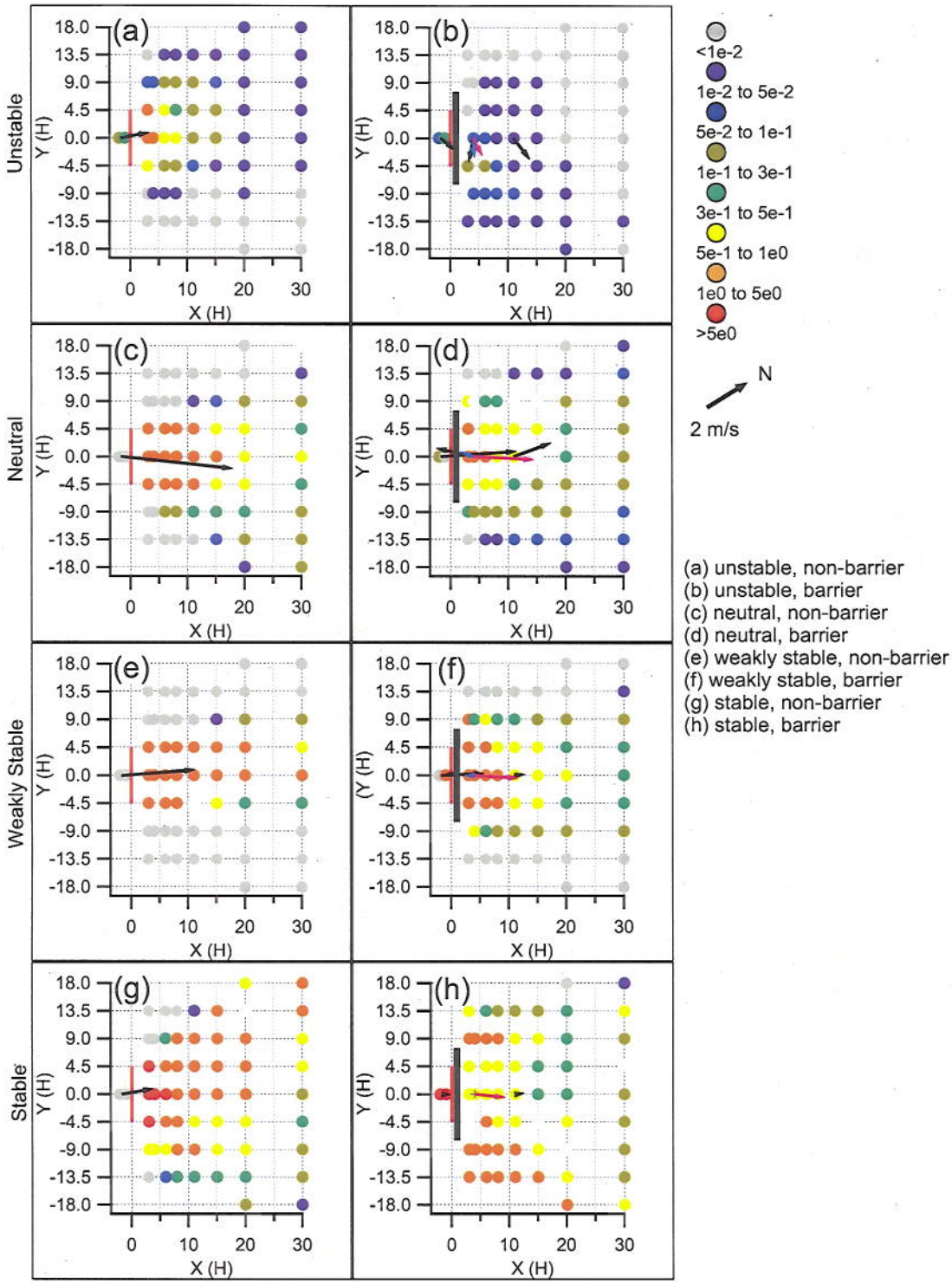
Unstable
Neutral
Weakly Stable
Stable
(a)
(b)
(c)
(d)
(e)
(f)
(g)
(h)
Y (H)
X (H)
18.0
13.5
9.0
4.5
0.0
-4.5
-9.0
-13.5
-18.0
0
10
20
30
<1e-2
1e-2 to 5e-2
5e-2 to 1e-1
1e-1 to 3e-1
3e-1 to 5e-1
5e-1 to 1e0
1e0 to 5e0
>5e0
N
2 m/s
(a) unstable, non-barrier
(b) unstable, barrier
(c) neutral, non-barrier
(d) neutral, barrier
(e) weakly stable, non-barrier
(f) weakly stable, barrier
(g) stable, non-barrier
(h) stable, barrier

Figure 5

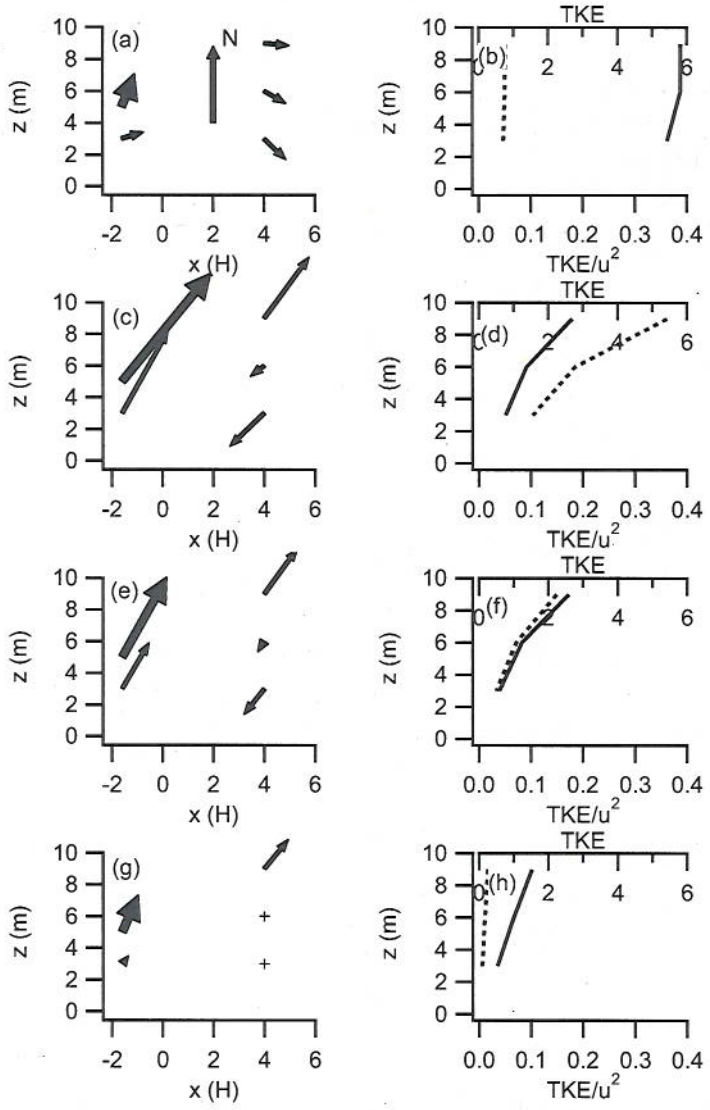

535
536 Figure 6

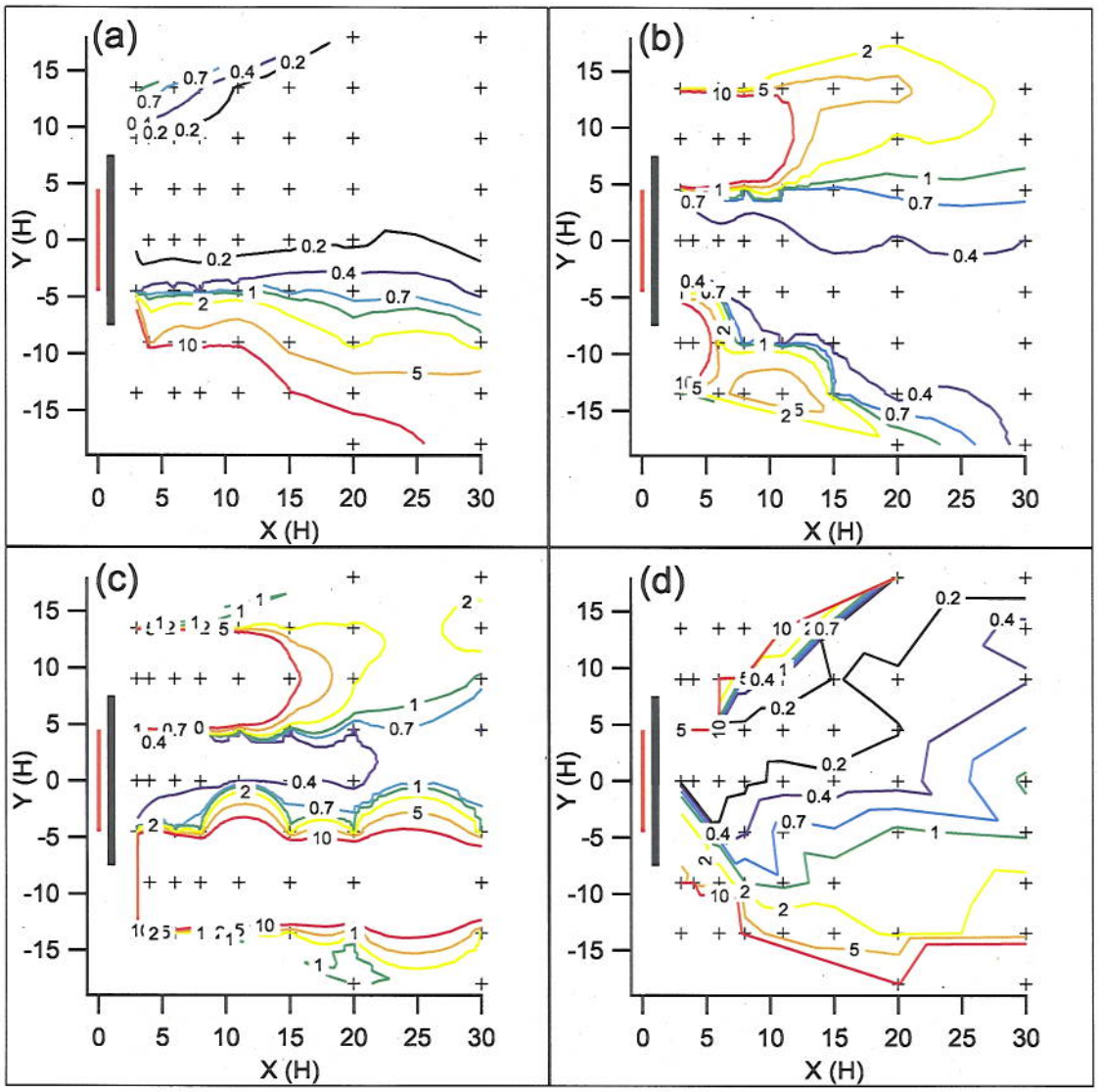

Figure 7

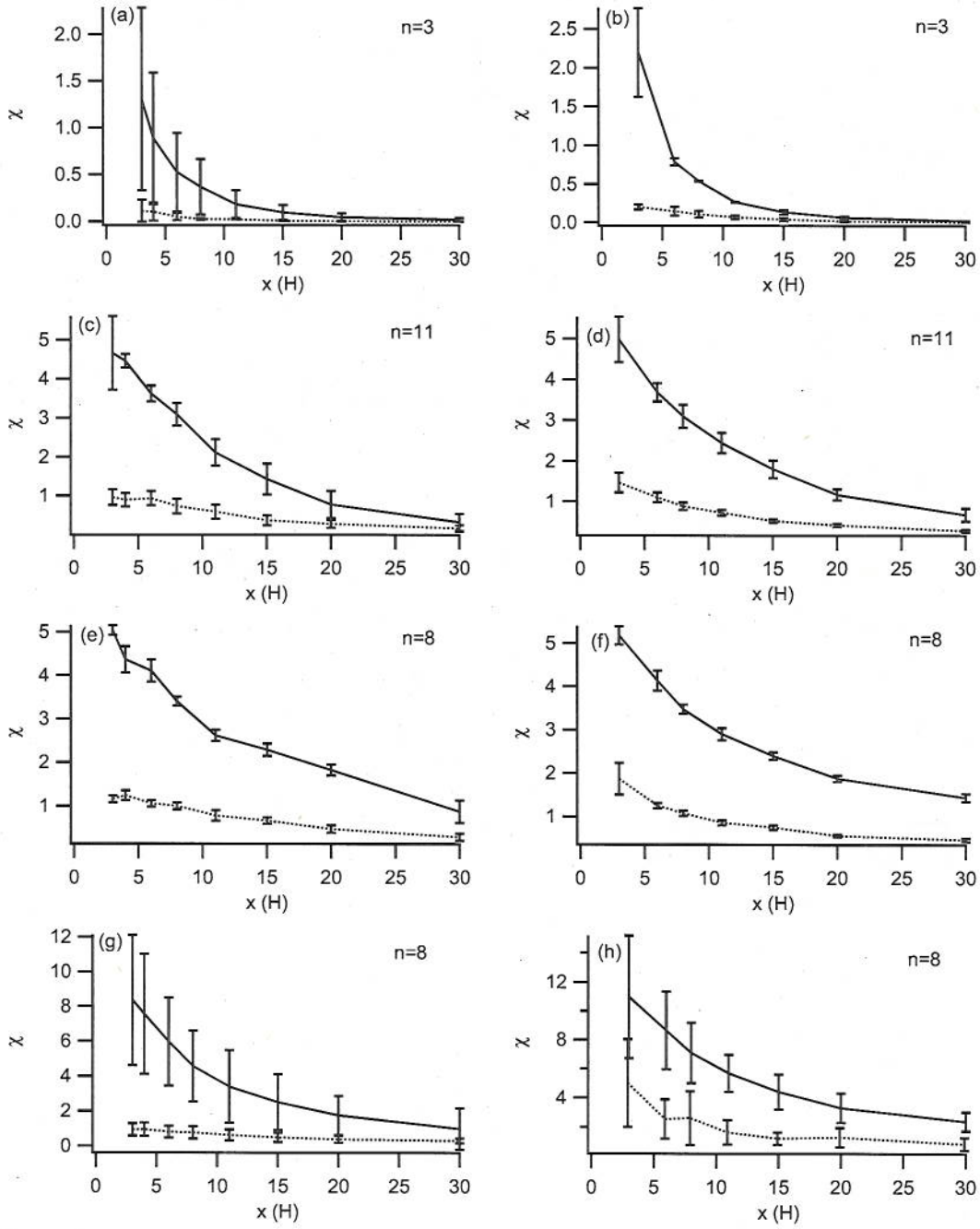

Figure 8

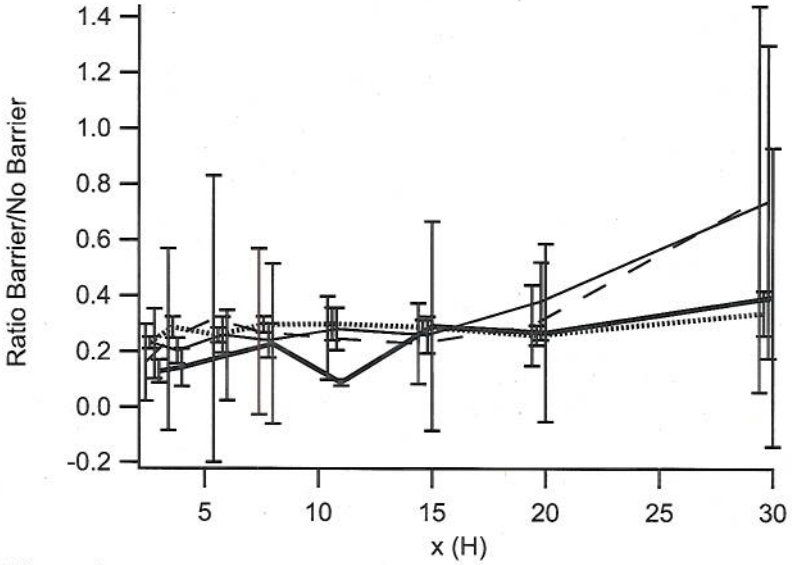

545
546 Figure 9

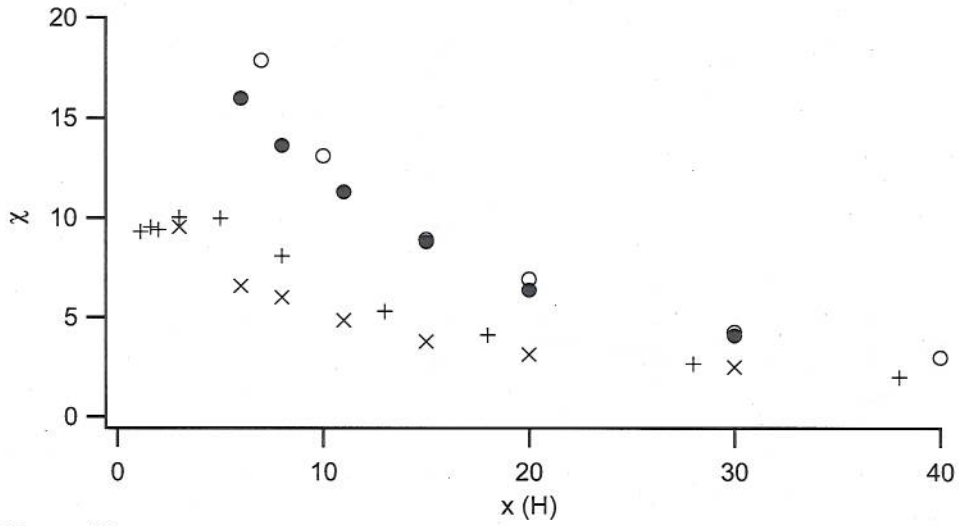

Figure 10

549 List of Figures
550
551 Figure 1. Mock straw bale sound barrier, 6 m high and 90 m long.
552
553 Figure 2. Schematic map of the primary sampling grid with locations of the anemometers (×),
554 line source release (solid line), barrier (bold line), and tracer samplers (•). The anemometer
555 indicated at x = 4H represents a tower with anemometers at z = 3, 6, and 9 m.
556
557 Figure 3. Photo of bag samplers and anemometers at x = 4H (tower) and 11H downwind of the
558 barrier.
559
560 Figure 4. Diagram of the SF_6 release system.
561
562 Figure 5. Corresponding non-barrier (left column) and barrier (right column) normalized tracer
563 concentration/wind vector maps for representative (a, b) unstable, (c, d) neutral, (e, f) weakly
564 stable, and (g, h) stable cases. Tracer release line is shown in bright red; the barrier in bold
565 black. Wind vector heights are color coded as described in text.
566
567 Figure 6. Wind vector and turbulence profile plots for the selected 15-min periods. Profiles for
568 TKE (dashed) and normalized TKE (solid) are shown for the tower at x = 4H. Unstable (a, b);
569 neutral (c, d); weakly stable (e, f); and stable (g, h). The reference north arrow (N) wind vector
570 in (a) has magnitude of 3 m s^{-1}. The '+' denotes less than 0.4 m s^{-1}. Bold wind vector represents
571 the reference wind from the control experiment.
572
573 Figure 7. Contour maps of the ratio between barrier and non-barrier tracer concentrations at
574 corresponding grid locations for the selected (a) unstable, (b) neutral, (c) weakly stable, and (d)
575 stable cases. Tracer release line (bright red) and barrier (bold black) are shown for reference.
576
577 Figure 8. Mean normalized concentration profiles for centerline (left column) and crosswind
578 maxima (right column) for qualifying 15-min periods. Unstable (a, b), neutral (c, d), weakly
579 stable (e, f), and stable (g, h) results for non-barrier (solid) and barrier (dashed) cases. Error bars
580 are the standard deviations. Number of qualifying periods given by n.
581
582 Figure 9. Mean barrier/non-barrier normalized centerline concentration ratios for qualifying
583 periods: unstable, bold; neutral, solid; weakly stable, dotted; stable, dashed. Error bars are
584 standard deviations.
585
586 Figure 10. Comparison between field and wind tunnel results for representative neutral case (•
587 field, no barrier; ○ wind tunnel, no barrier; × field, barrier; + wind tunnel, barrier).
588

589

Test	z/L	Stability	P-G	WS ($m\ s^{-1}$)	WD (deg)	u_* ($m\ s^{-1}$)	H ($W\ m^{-2}$)	σ_θ (deg)
2	-0.312	Unstable	B	1.4	201	0.29	200.0	28.8
1	-0.016	Neutral	D	5.5	219	0.55	73.4	11.4
3	0.048	Weakly stable	D	3.6	209	0.35	-54.1	8.7
5	0.379	Strongly stable	F	1.6	203	0.12	-15.2	8.5

590

591 Table 1. Meteorological approach flow conditions at the non-barrier reference anemometer at x
592 = -1.6H, z = 3 m for the selected 15-min cases. P-G is the Pasquill-Gifford stability class
593 determined by the Solar Radiation Delta-T (SRDT) method (EPA 2000).

594

595

Measurement	Test	x = -1.6H z = 3 m*	x = -1.6H z = 3 m	x = 4H z = 3 m	x = 4H z = 6 m	x = 4H z = 9 m	x = 11H z = 3 m
WS ($m\ s^{-1}$)	2	1.4	0.9	1.2	1.0	1.0	1.3
	1	5.5	3.7	1.9	0.7	3.0	2.0
	3	3.6	2.1	1.3	0.5	2.2	0.5
	5	1.6	0.4	0.3	0.1	1.5	0.5
WD (deg)	2	201	253	314	300	276	265
	1	219	209	46	52	216	193
	3	209	210	38	32	216	206
	5	203	216	41	214	219	207
u_* ($m\ s^{-1}$)	2	0.29	0.23	0.28	0.35	0.36	0.19
	1	0.55	0.61	0.17	0.31	1.28	0.72
	3	0.35	0.37	0.13	0.22	0.85	0.34
	5	0.12	0.09	0.03	0.20	0.24	0.18
TKE ($m^2\ s^{-2}$)	2	0.73	0.54	0.71	0.76	0.76	0.81
	1	2.36	2.07	1.55	2.77	5.43	4.86
	3	0.58	0.69	0.50	1.07	2.24	1.14
	5	0.21	0.08	0.09	0.17	0.26	0.34

596 Table 2. Wind field and turbulence measurements for the selected 15-min cases at the 5 barrier
597 grid sonic anemometers and one non-barrier (*) reference sonic anemometer.
598